Bandpass Filtering Power Amplifier With Wide Stopband and High Out-of-Band Rejection

Shaobo Li, Yongle Wu, *Senior Member, IEEE*, Yuhao Yang, Xiaopan Chen, Weimin Wang, *Senior Member, IEEE*, and Zhuoyin Chen

***Abstract*—In this brief, a power amplifier (PA) with excellent integrated filtering characteristics is presented. The designed process is based on a novel impedance transformer (IT) consisting of cascaded coupled-line sections with stubs. The proposed IT generates four transmission zeros (TZs), which not only greatly improves the frequency selectivity, but also improves the second harmonic suppression performance, further enhancing the linearity of the PA. For demonstration, a bandpass filtering PA is designed, fabricated, and measured. The designed PA exhibits both good filtering bandpass response and power amplification. The rejection levels are larger than 59.7 and 69 dB for the lower and higher suppression bands. Meanwhile, the measured drain efficiency (DE) of the constructed PA is 58.5%-73% with a large-signal gain of 8.9-10.2 dB at 1.85-2.1 GHz. Besides, using a 20 MHz long-term evolution signal as the driving signal for the PA, the adjacent channel power ratio is lower than −57.8 dBc.**

***Index Terms*—Bandpass, coupled-line, filtering, impedance transformer (IT), linearity, power amplifier (PA).**

I. Introduction

With the rapid development of communication systems, the wireless communication system (WLCS) mainly includes the baseband chip, radio frequency (RF) transceiver, RF front-end module, and antenna module. The RF front-end module is the core part of the WLCS, mainly including RF switches, low-noise amplifiers, filters, power dividers, and power amplifiers (PAs) [1], among which PAs and filters are core devices.

In general, bandpass filters (BPFs) are cascaded after PAs to suppress out-of-band signals. Nevertheless, in most cases, PAs and filters are independently designed based on 50 Ω systems. Therefore, impedance mismatches at the connection may affect the system performance to some extent. Under this circumstance, the co-designs of PAs and filters have drawn the attention of many researchers. Impedance transformers (ITs) or filters with bandpass filtering characteristics are used as matching networks for PAs to replace cascaded filters. Therefore, system losses and mismatches can be reduced, and the overall system performance can be improved.

ITs with filtering characteristics have been proposed [2], [3], [4], [5], [6]. In [3], filtering ITs consisting of coupled lines achieve high transforming ratios and extremely high/low terminal real impedances. The complex IT is presented in [5]. Besides, the compact microstrip BPF is used as the output matching network (OMN) of the PA [7]. To improve the efficiency, harmonic suppression and Doherty PAs with bandpass response are proposed [8], [9], [10], [11]. In [8], the second harmonic tuned broadband PA with filtering characteristics is presented and the maximum efficiency of the PA can achieve 65%. In the Doherty PA design [10], the conventional input power divider is replaced by a quadrature coupler with bandpass characteristics to realize the bandpass filtering response. Although the above-designed PAs can achieve high efficiency, the out-of-band suppression and frequency selectivity are poor. On the other hand, due to the high-Q factor of the cavity and dielectric resonator [12], [13], [14], losses can be further reduced and roll-off characteristics can be improved. Based on the dielectric resonator (DR) [12] and the hybrid cavity filter [13], the designed PAs show excellent filtering characteristics, and the efficiency can achieve 70.7% and 75.5%, respectively. Nevertheless, cavity filters and DRs are more complex to implement, while microstrip technology allows for smaller and simpler circuits.

In this brief, based on the proposed bandpass filtering IT (BFIT), the PA with integrated filtering characteristics is designed and exhibits the following advantages: 1) wide stopband; 2) high out-of-band suppression levels; 3) harmonic suppression; 4) excellent linearity; 5) inherent DC block; 6) simple structure and easy implementation.

II. Design and Analysis of the Proposed BFIT

Fig. 1 illustrates the topology of the proposed BFIT, which contains three basic blocks (block I, II, and III). Block I consists of two cascaded transmission-line (TL1 and TL2) sections. Block II is comprised of the coupled-line (CL1), where ports 2 and 4 are open. Block III is composed of the coupled-line (CL2) with the short-circuited stub (TL3). The even- and odd-mode impedances of coupled lines are represented by

Manuscript received 19 August 2022; revised 10 October 2022; accepted 26 October 2022. Date of publication 8 November 2022; date of current version 6 March 2023. This work was supported in part by the National Natural Science Foundation of China under Grant 61971052, Grant U21A20510, and Grant U20A20203; and in part by the Key Research and Development Project of Guangdong Province under Grant 2020B0101080001. This brief was recommended by Associate Editor C. Condo. *(Corresponding author: Yongle Wu.)*

Shaobo Li, Yongle Wu, Yuhao Yang, Xiaopan Chen, and Zhuoyin Chen are with the School of Integrated Circuits, Beijing University of Posts and Telecommunications, Beijing 100876, China (e-mail: bsl_2000@bupt.edu.cn; wuyongle138@gmail.com; yangyuhao1996@gmail.com; chenxiaopan@bupt.edu.cn; chenzhuoyin001@gmail.com).

Weimin Wang is with the School of Electronic Engineering, Beijing University of Posts and Telecommunications, Beijing 100876, China (e-mail: wangwm@bupt.edu.cn).

Color versions of one or more figures in this article are available at https://doi.org/10.1109/TCSII.2022.3220619.

Digital Object Identifier 10.1109/TCSII.2022.3220619

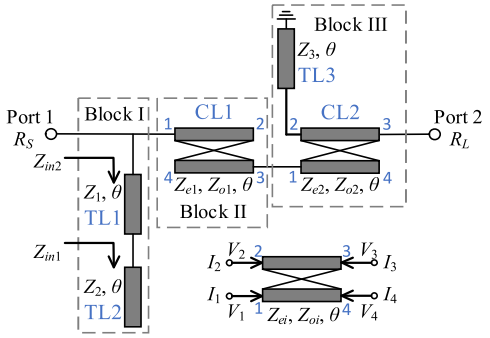

Fig. 1. Topology of the proposed bandpass filtering impedance transformer.

Z_{ei} and Z_{oi} (i =1, 2), whereas electrical length is denoted with θ. The characteristic impedances and electrical lengths of three transmission lines are represented by Z_i (i = 1, 2, 3) and θ. Based on the *ABCD* matrix of the two-port network, the three basic blocks are first analyzed, and then the circuit characteristics of the overall structure are analyzed and interpreted.

According to the microwave network theory and the circuit theory, the *ABCD* matrix of block I is given as (1) and (2).

$$\begin{bmatrix} A_{\rm I} & B_{\rm I} \\ C_{\rm I} & D_{\rm I} \end{bmatrix} = \begin{bmatrix} 1 & 0 \\ Y_{in2} & 1 \end{bmatrix} \tag{1}$$

$$\begin{cases} Z_{in1} = -jZ_2/\tan(\theta) \\ Z_{in2} = Z_1 \dfrac{Z_{in1} + jZ_1\tan(\theta)}{Z_1 + jZ_{in1}\tan(\theta)} \\ Y_{in2} = 1/Z_{in2} \end{cases} \tag{2}$$

Assuming

$$Z_{ai} = Z_{ei} + Z_{oi}, Z_{bi} = Z_{ei} - Z_{oi} (i = 1, 2), \tag{3}$$

we obtain the *Z*-parameters of the 4-port coupled-line given in (4) and (5). Block II is limited by the current ($I_2 = I_4 = 0$). Block III is limited by the voltage ($U_2 = j2U_0\sin(\theta)$) and current ($I_2 = -2U_0\cos(\theta)/Z_3$ and $I_4 = 0$). Therefore, the 4-port network can be converted to the 2-port network [15]. Here U_0 is just an intermediate variable.

$$\begin{cases} U_1 = Z_{11}I_1 + Z_{12}I_2 + Z_{13}I_3 + Z_{14}I_4 \\ U_2 = Z_{21}I_1 + Z_{22}I_2 + Z_{23}I_3 + Z_{24}I_4 \\ U_3 = Z_{31}I_1 + Z_{32}I_2 + Z_{33}I_3 + Z_{34}I_4 \\ U_4 = Z_{41}I_1 + Z_{42}I_2 + Z_{43}I_3 + Z_{44}I_4 \end{cases} \tag{4}$$

$$\begin{cases} Z_{11} = Z_{22} = Z_{33} = Z_{44} = -jZ_{ai}\cot(\theta)/2 \\ Z_{12} = Z_{21} = Z_{34} = Z_{43} = -jZ_{bi}\cot(\theta)/2 \\ Z_{13} = Z_{24} = Z_{31} = Z_{42} = -jZ_{bi}\csc(\theta)/2 \\ Z_{14} = Z_{41} = Z_{23} = Z_{32} = -jZ_{ai}\csc(\theta)/2 \end{cases} \tag{5}$$

The *ABCD* matrices or parameters of blocks II and III are derived as (6) and (7), respectively.

$$\begin{bmatrix} A_{\rm II} & B_{\rm II} \\ C_{\rm II} & D_{\rm II} \end{bmatrix} = \begin{bmatrix} \dfrac{Z_{a1}\cos(\theta)}{Z_{b1}} & \dfrac{j(Z_{b1}^2 - Z_{a1}^2\cos^2(\theta))}{2Z_{b1}\sin(\theta)} \\ \dfrac{j2\sin(\theta)}{Z_{b1}} & \dfrac{Z_{a1}\cos(\theta)}{Z_{b1}} \end{bmatrix} \tag{6}$$

$$\begin{cases} A_{\rm III} = \dfrac{((Z_{b2}^2 - Z_{a2}^2)\cot^2(\theta) + 2Z_3Z_{a2})\cos(\theta)}{2Z_3Z_{b2}} \\ B_{\rm III} = j\dfrac{(2Z_3 + Z_{a2}\cos^2(\theta))Z_{b2}^2 - Z_mZ_{a2}^2\cos^2(\theta)}{4Z_3Z_{b2}\sin(\theta)} \\ C_{\rm III} = j\dfrac{(2Z_3 - Z_{a2}\cot^2(\theta))\sin(\theta)}{Z_3Z_{b2}} \\ D_{\rm III} = \dfrac{Z_mZ_{a2}\cos(\theta)}{2Z_3Z_{b2}}, Z_m = 2Z_3 + Z_{a2} \end{cases} \tag{7}$$

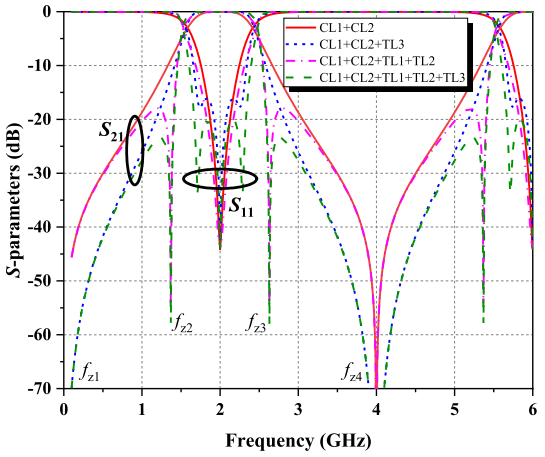

Fig. 2. Ideal simulated *S*-parameters corresponding to the BFIT for four cases (R_S = 10 Ω).

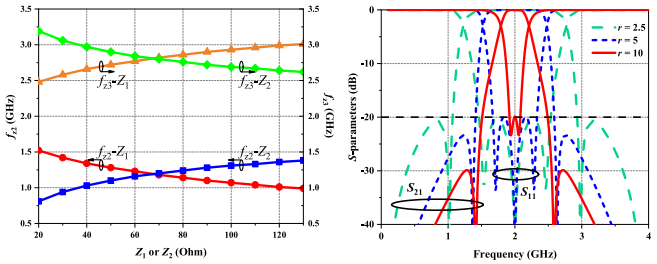

(a) (b)

Fig. 3. (a) Variations of two transmission zeros (f_{z2} and f_{z3}) under different values of Z_1 or Z_2, respectively. (b) 3-dB fractional bandwidth of the BFIT under different r.

Combining (1)-(2) and (6)-(7), the *ABCD* parameters of the BFIT can be derived as (8), and detailed results are given in (9), shown at the bottom of the next page, (10).

$$\begin{cases} A_{\rm t} = (A_{\rm I}A_{\rm II} + B_{\rm I}C_{\rm II})A_{\rm III} + (A_{\rm I}B_{\rm II} + B_{\rm I}D_{\rm II})C_{\rm III} \\ B_{\rm t} = (A_{\rm I}A_{\rm II} + B_{\rm I}C_{\rm II})B_{\rm III} + (A_{\rm I}B_{\rm II} + B_{\rm I}D_{\rm II})D_{\rm III} \\ C_{\rm t} = (A_{\rm II}C_{\rm I} + C_{\rm II}D_{\rm I})A_{\rm III} + (B_{\rm II}C_{\rm I} + D_{\rm I}D_{\rm II})C_{\rm III} \\ D_{\rm t} = (A_{\rm II}C_{\rm I} + C_{\rm II}D_{\rm I})B_{\rm III} + (B_{\rm II}C_{\rm I} + D_{\rm I}D_{\rm II})D_{\rm III} \end{cases} \tag{8}$$

$$\begin{cases} Z_{m1} = Z_{a1}(Z_{a1} + Z_{a2})\cos^2(\theta) - Z_{b1}^2 \\ Z_{m2} = Z_{b2}^2(2Z_3 + Z_{a2}\cos^2(\theta)) \\ Z_{m3} = Z_{a1} - \dfrac{(Z_1+Z_2)(Z_{a1}^2\cot^2(\theta) - Z_{b1}^2\csc^2(\theta))}{2Z_1(Z_1 - Z_2\cot^2(\theta))} \\ Z_{m4} = 2\sin(\theta) + \dfrac{Z_{a1}(Z_1+Z_2)\cos(\theta)\cot(\theta)}{Z_1(Z_2\cot^2(\theta) - Z_1)} \end{cases} \tag{10}$$

Assuming the impedance transformer ratio $r = R_L/R_S$ ($R_L > R_S$), the *S*-parameters of the proposed BFIT can be derived as (11) by converting the *ABCD* matrix to the *S* matrix.

$$\begin{cases} S_{11} = \dfrac{A_{\rm t}rR_S + B_{\rm t} - C_{\rm t}rR_S^2 - D_{\rm t}R_S}{A_{\rm t}rR_S + B_{\rm t} + C_{\rm t}rR_S^2 + D_{\rm t}R_S} \\ S_{21} = \dfrac{2R_S\sqrt{r}}{A_{\rm t}rR_S + B_{\rm t} + C_{\rm t}rR_S^2 + D_{\rm t}R_S} \end{cases} \tag{11}$$

When θ is equal to 90°, for matching at the frequency f_0, the magnitude of S_{11} should be equal to 0.

Fig. 2 depicts the simulated *S*-parameters corresponding to the BFIT for four cases. TL1 and TL2 can generate two extra transmission zeros (TZs) (f_{z2} and f_{z3}) and TL3 can generate two extra transmission poles (TPs), which greatly increases the frequency selectivity and roll-off skirt across the

TABLE I
THE OPTIMIZED CIRCUIT PARAMETERS IN FIG. 2 AND FIG. 3

	r	Z_{e1} (Ω)	Z_{e2} (Ω)	Z_{o1} (Ω)	Z_{o2} (Ω)	Z_1 (Ω)	Z_2 (Ω)	Z_3 (Ω)
Fig. 2 Fig. 3(b)	5	63	105.5	33	38	36.5	125	39
Fig. 3(a)						20~130	20~130	
Fig. 3(b)	2.5	89.5	123	32.5	32	58	61.5	134.5
	10	51.5	81	37.5	41	26	105.5	72.5

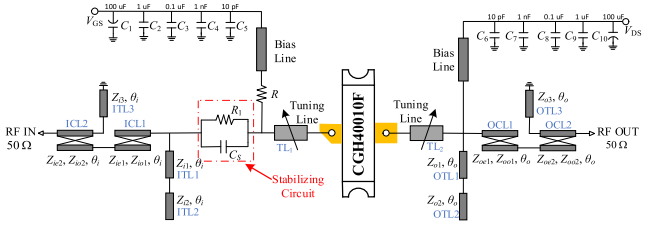

Fig. 4. The schematic of the designed filtering power amplifier.

passband. Besides, TL1 and TL2 jointly control the positions of two extra TZs. Fig. 3(a) shows variations of f_{z2} and f_{z3} with different characteristic impedances Z_1 and Z_2 when other parameters are fixed. Fig. 3(b) presents that 3-dB fractional bandwidth (FBW) can be achieved for 76%, 48%, and 22% under the same return loss (RL = 20 dB) and different r. The initially required parameters are listed in Table I.

III. DESIGN AND ANALYSIS OF THE FILTERING PA

The ideal schematic of the filtering PA is shown in Fig. 4. The selected transistor for the PA design is a 10-watt gallium nitride (GaN) HEMT CGH40010F, which has been biased in a class-AB mode. The input matching network (IMN) and OMN are constructed by the proposed BFIT. R_1 = 39 Ω, C_S = 3.6 pF, and R = 47 Ω are used to improve the stability of the PA. The simulated and measured stability factors K are shown in Fig. 9(b) and are greater than 1. The tuning line TL_1 is used to remove the imaginary part of the optimal source impedance [9], and the tuning line TL_2 is combined with the proposed BFIT to match the optimal load impedance. Besides, tuning lines TL_1 and TL_2 are used as transistor pads. Meanwhile, to prevent damage to the power supply caused by RF signals, quarter-wavelength lines are used in the gate and drain bias circuits. The specific design process of the filtering PA is addressed as follows.

A. Source-Pull and Load-Pull Analysis

Fig. 5(a) and (b) exhibits results of source-pull without and with TL_1 at the fundamental frequency from 1.8-2.1 GHz (power added efficiency (PAE) > 65% and output power (P_{out}) > 40 dBm). The optimal source impedance is complex in Fig. 5(a). Due to the proposed real-real BFIT, its imaginary

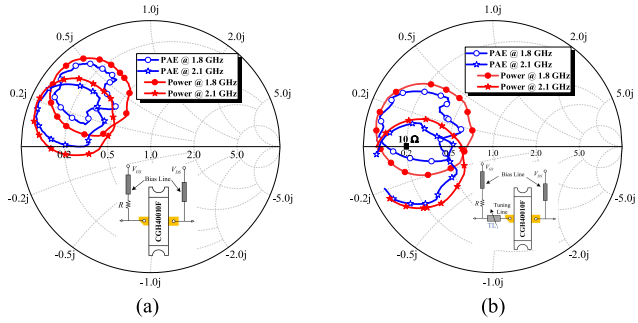

Fig. 5. Simulated source-pull results across 1.8-2.1 GHz (a) without (b) with the tuning line (TL_1).

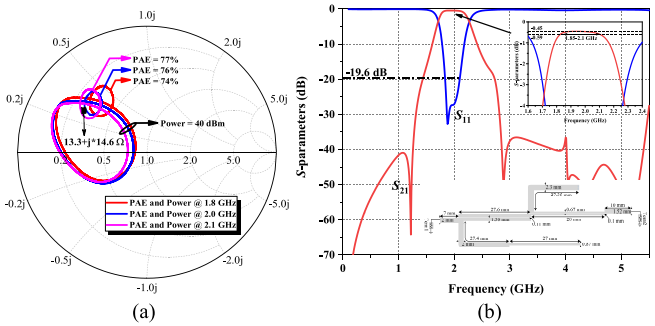

Fig. 6. (a) Simulated load-pull results at the fundamental frequency. (b) The simulated results of the OMN.

part can be removed by TL_1 in Fig. 5(b). The characteristic impedance and electrical length of TL_1 are optimized as 30.8 Ω and 22° at the operating frequency f_0 = 2 GHz. Fig. 6(a) shows load-pull results (PAE > 74% and P_{out} > 40 dBm). Besides, the optimal source and load impedances are used for matching network designs, which is critical for the design of the PA. Therefore, to make a trade-off between PAE and P_{out}, Z_{Iopt} = 10 Ω and Z_{Oopt} = (13.3 + j14.6) Ω are chosen as the optimal source and load impedances.

B. Matching Networks Design

To achieve the excellent matching effect at the operating band, terminal impedances of the IMN and OMN are chosen as (Z^*_{Iopt}, 50 Ω) and (Z^*_{Oopt}, 50 Ω), respectively. The parameter values of the IMN and OMN are optimized as: Z_{ie1} = 65.5 Ω, Z_{ie2} = 99 Ω, Z_{io1}= Z_{io2} =37.5 Ω, Z_{i1}= 30.5 Ω, Z_{i2}= 79.5 Ω, Z_{i3} = 41.5 Ω, Z_{oe1}= 66.5 Ω, Z_{oe2}= 97 Ω, Z_{oo1}= 37.5 Ω, Z_{oo2}= 37 Ω, Z_{o1}= 31 Ω, Z_{o2}= 76.5 Ω, Z_{o3}= 33.5 Ω, and θ_i = θ_o = 90°. Besides, the 40 Ω tuning line (TL_2) with an electrical length of 22° is connected with the OMN. Fig. 6(b) shows the simulated results of the OMN. In 1.85-2.1 GHz, the minimum and maximum insertion loss are 0.45 dB and 0.59 dB, and the return loss is greater than 19.6 dB.

$$\begin{cases} A_t = \dfrac{Z_{m1}(2Z_3 - Z_{a2}\cot^2(\theta)) + Z_{a1}Z_{b2}^2\cos^2(\theta)\cot^2(\theta)}{2Z_3Z_{b1}Z_{b2}},\ B_t = \dfrac{-j\cot(\theta)}{4Z_3Z_{b1}Z_{b2}}(Z_{a2}Z_mZ_{m1} - Z_{a1}Z_{m2}) \\ C_t = \dfrac{j\cos(\theta)}{2Z_3Z_{b1}Z_{b2}}(2Z_{m3}(2Z_3 - Z_{a2}\cot^2(\theta))\sin(\theta) + Z_{m4}(Z_{b2}^2 - Z_{a2}^2)\cot^2(\theta) + 2Z_3Z_{a2}Z_{m4}) \\ D_t = \dfrac{1}{4Z_3Z_{b1}Z_{b2}}(Z_{a2}^2Z_mZ_{m4}\cos(\theta)\cot(\theta) - Z_{m2}Z_{m4}\csc(\theta) + 2Z_{a2}Z_mZ_{m3}\cos^2(\theta)) \end{cases} \quad (9)$$

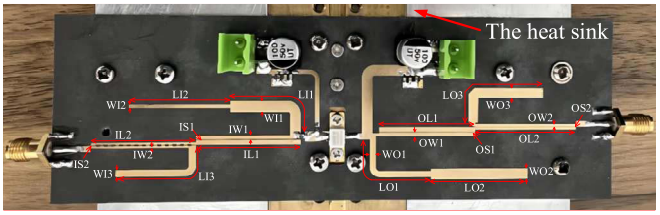

Fig. 7. Photograph of the designed filtering PA. (IW1 = 1.23, IS1 = 0.19, IL1 = 28, IW2 = 0.65, IS2 = 0.15, IL2 = 27.6, WI1 = 2.9, LI1 = 25.5, WI2 = 0.9, LI2 = 27, WI3 = 1.9, LI3 = 26.4, OW1 = 1.3, OS1 = 0.11, OL1 = 26.5, OW2 = 0.7, OS2 = 0.1, OL2 = 28.2, WO1 = 1.7, LO1 = 26.4, WO2 = 3, LO2 = 26.9, WO3 = 2.64, LO3 = 27 (unit: mm)).

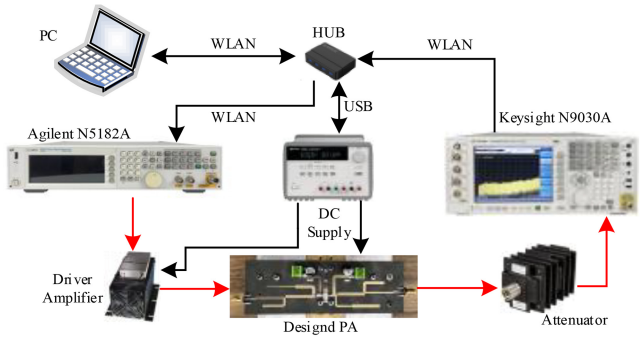

Fig. 8. Experimental setup.

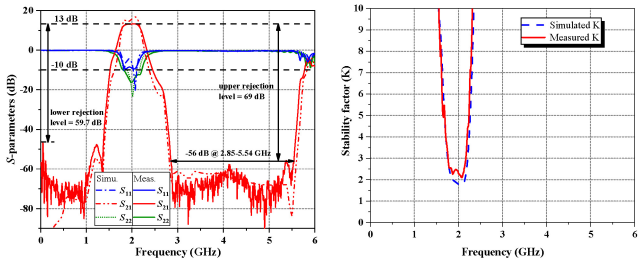

(a) (b)

Fig. 9. (a) EM simulated and measured *S*-parameters of the designed filtering PA. (b) EM simulated and measured stability factors K of the PA.

C. EM Simulation and Measurement

To better verify the validity, based on parameters of the IMN and OMN, the filtering PA is optimized, electromagnetic (EM) simulated, and fabricated on the substrate of RT/Duroid 5880 with a relative permittivity $\varepsilon_r = 2.2$, a thickness $h = 0.508$ mm, and a loss tan $\sigma = 0.0009$. The layout and main physical dimensions of the PA are shown in Fig. 7. The drain and gate bias voltages are set to $V_{DS} = 28$ V and $V_{GS} = -2.9$ V, and the quiescent drain current (I_D) is 106 mA. Ten capacitors (C_1-C_{10}) are used to remove noise from the DC power supply. EM simulation is performed by using the EM simulator Advanced Design System.

Fig. 8 shows the test environment. The small-signal *S*-parameters of the PA measured by using an Agilent N5230C vector network analyzer are shown in Fig. 9(a). In the designed frequency band, the minimum small-signal gain is 11.8 dB and the maximum is 13 dB. Besides, the measured lower and upper stopband rejection levels are larger than

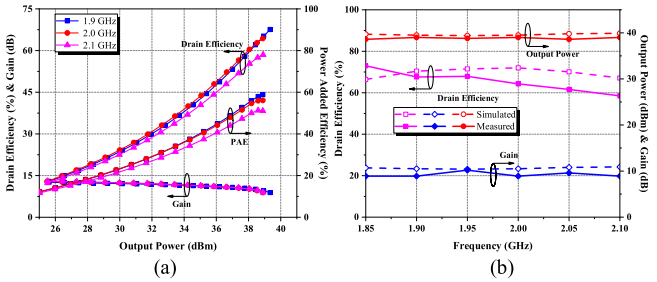

(a) (b)

Fig. 10. EM simulated and measured results of the designed filtering PA versus (a) output power and (b) frequency.

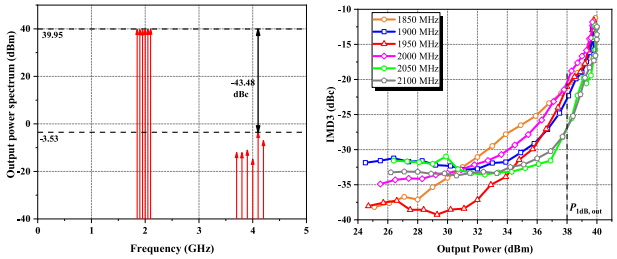

(a) (b)

Fig. 11. (a) Measured output power spectrum at saturation (fundamental and second harmonic) of the PA. (b) Measured IMD3 of the PA.

59.7 dB (DC-1.37 GHz) and 69 dB (2.85-5.54 GHz), respectively. Meanwhile, due to additional TZs, the overall rolling skirt through the passband becomes sharper and the stopband is wider. The experimental results show that the fundamental impedance is well matched and the second harmonic is highly suppressed. The simulated and measured deviations of S_{21} are mainly attributed to the fabrication tolerance and the nominal error of the materials.

Fig. 10(a) depicts the measured drain efficiency (DE), PAE, and gain versus output power by a continuous wave signal from 1.9-2.1 GHz (frequency step is 100 MHz). Fig. 10(b) shows that the measured DE, P_{out}, and gain are 58.5%-73%, 38.6-39 dBm, and 8.9-10.2 dB at the saturation level. There is a big difference between the simulated and measured DE, and the main reasons are manufacturing errors, measurement errors, and deviations in the transistor model. Fig. 11(a) shows the measured output power spectrum of the fundamental and second harmonic at saturation, and the second harmonic is better suppressed (output power < -3.53 dBm). On the other hand, the linearity is measured by using a two-tone signal with a frequency spacing of 10 MHz, and Fig. 11(b) illustrates the measured third-order intermodulation distortions (IMD3) is below -20.4 dBc at the 1-dB compression point. Besides, Fig. 12 shows the measured output spectrum without and with the digital predistortion (DPD) technique by using a 20 MHz long-term evolution (LTE) signal at 1.95 GHz. The adjacent channel power ratio (ACPR) is improved from -34.8 dBc to -57.8 dBc when DPD is applied.

The performance comparisons of this brief and prior PAs are listed in Table II. Although PAs in [12] and [16] realize high efficiency, their working bandwidth is narrow. Besides, in [16], the PA does not show the bandpass filtering response. Compared with the designed PAs

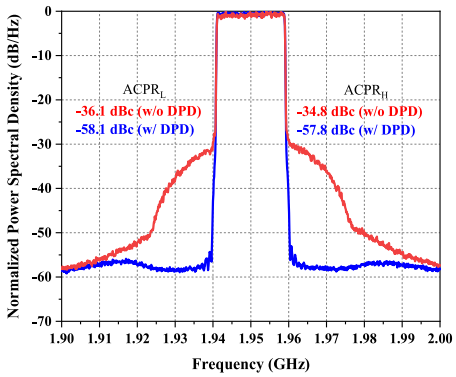

Fig. 12. The output spectrum of the designed filtering PA with and without DPD.

TABLE II
THE PERFORMANCE COMPARISON OF FILTERING PAS

Refs.	Frequency (GHz)	Filter Type	BFR	SRL (dB)	Eff_M (%)	IMD3 (dBc)	ACPR (dBc)
[12]	1.88	DR BPF	Yes	> 25*	70.7 (P)	N.A.	N.A.
[14]	2.95-3.35	Cavity BPF	Yes	> 22*	67 (D)	N.A.	N.A.
[16]	2.4	Microstrip LPF	No	-	74 (P)	N.A.	N.A.
[17]	2.57-2.67	Microstrip BPF	Yes	> 20	46.3 (P)	N.A.	N.A.
[18]	5.4-5.6	SIW FB	Yes	> 40*	48.7 (P)	N.A.	N.A.
[19]	0.8-1	SISL BPF	Yes	> 53.7	57.5 (D)	< -26	N.A.
[10]	1.72-1.85	BQ coupler	Yes	> 40.7	41.8 (P)	N.A.	N.A.
This work	1.85-2.1	Microstrip BFIT	Yes	> 59.7	73 (D)	< -20.4	< -57.8

BFR: Bandpass Filtering Response; SRL: Stopband Rejection Level; Eff_M: Maximum Efficiency; P: PAE; D: DE; SIW: Substrate integrated waveguide; FB: Filtering Balun; SISL: Substrate integrated suspended line; BQ: Bandpass quadrature; *: estimated value.

in [10], [14], [17], [18], [19], due to two extra TZs, the designed filtering PA exhibits sharper roll-off across the passband, higher out-of-band rejection levels, higher efficiency, and better harmonic suppression. However, the BFIT composed of coupled lines brings a larger loss, and as the frequency rises, the loss increases rapidly. Besides, the power handling capability of the microstrip line structure is not excellent. In contrast, SIW, DR, and waveguide filters with high-Q factors, low losses, and high-power handling capabilities are widely used in filtering PA designs.

IV. CONCLUSION

This brief has presented a high-efficiency filtering PA with wide stopbands and high out-of-band rejection levels. Based on the microwave and circuit theory, the frequency selective characteristics and two extra transmission zeros positions of the proposed BFIT are analyzed. By adding stubs, two extra generated transmission zeros greatly improve roll-off characteristics. The linearity of the PA is greatly improved due to the better harmonic rejection characteristics, and the ACPR can achieve −57.8 dBc with DPD. Besides, the maximum DE of the PA can reach 73%, exhibiting excellent power amplification characteristics. Based on PCB technology, the filtering PA can also be easily implemented and fabricated.

REFERENCES

[1] Z. Zhuang, Y. Wu, Q. Yang, M. Kong, and W. Wang, "Broadband power amplifier based on a generalized step-impedance Quasi-Chebyshev low-pass matching approach," *IEEE Trans. Plasma Sci.*, vol. 48, no. 1, pp. 311–318, Jan. 2020.

[2] P. Kim, G. Chaudhary, and Y. Jeong, "Ultra-high transforming ratio coupled line impedance transformer with bandpass response," *IEEE Microw. Wireless Compon. Lett.*, vol. 25, no. 7, pp. 445–447, Jul. 2015.

[3] Y. Jeong, G. Chaudhary, and P. Kim, "Frequency selective impedance transformer with high-impedance transforming ratio and extremely high/low termination impedances," *IEEE Trans. Circuits Syst. I, Reg. Papers*, vol. 68, no. 6, pp. 2382–2392, Jun. 2021.

[4] W. Chen, Y. Wu, and W. Wang, "Planar wideband high-selectivity impedance-transforming differential bandpass filter with deep common-mode suppression," *IEEE Trans. Circuits Syst. II, Exp. Briefs*, vol. 67, no. 10, pp. 1914–1918, Oct. 2020.

[5] S. Fang, X. Jia, H. Liu, and Z. Wang, "Design of compact coupled-line complex impedance transformers with the series susceptance component," *IEEE Trans. Circuits Syst. II, Exp. Briefs*, vol. 67, no. 11, pp. 2482–2486, Nov. 2020.

[6] B. Zhang, Y. Wu, and Y. Liu, "Wideband single-ended and differential bandpass filters based on terminated coupled line structures," *IEEE Trans. Microw. Theory Techn.*, vol. 65, no. 3, pp. 761–774, Mar. 2017.

[7] L. Gao, X. Y. Zhang, S. Chen, and Q. Xue, "Compact power amplifier with bandpass response and high efficiency," *IEEE Microw. Wireless Compon. Lett.*, vol. 24, no. 10, pp. 707–709, Oct. 2014.

[8] M. F. Haider, F. You, T. Qi, C. Li, and S. Ahmad, "Co-design of second harmonic-tuned power amplifier and a parallel-coupled stub loaded resonator," *IEEE Trans. Circuits Syst. II, Exp. Briefs*, vol. 67, no. 12, pp. 3013–3017, Dec. 2020.

[9] Z. Zhuang, Y. Wu, M. Kong, and W. Wang, "High-selectivity single-ended/balanced DC-block filtering impedance transformer and its application on power amplifier," *IEEE Trans. Circuits Syst. I, Reg. Papers*, vol. 67, no. 12, pp. 4360–4369, Dec. 2020.

[10] S. Y. Zheng, Z. W. Liu, Y. M. Pan, Y. Wu, W. S. Chan, and Y. Liu, "Bandpass filtering Doherty power amplifier with enhanced efficiency and wideband harmonic suppression," *IEEE Trans. Circuits Syst. I, Reg. Papers*, vol. 63, no. 3, pp. 337–346, Mar. 2016.

[11] Z. Su, C. Yu, B. Tang, and Y. Liu, "Bandpass filtering power amplifier with extended band and high efficiency," *IEEE Microw. Wireless Compon. Lett.*, vol. 30, no. 2, pp. 181–184, Feb. 2020.

[12] J. Xu, X. Y. Zhang, and X.-Q. Song, "High-efficiency filter-integrated class-F power amplifier based on dielectric resonator," *IEEE Microw. Wireless Compon. Lett.*, vol. 27, no. 9, pp. 827–829, Sep. 2017.

[13] Q.-Y. Guo, X. Y. Zhang, J.-X. Xu, Y. C. Li, and Q. Xue, "Bandpass class-F power amplifier based on multifunction hybrid cavity-microstrip filter," *IEEE Trans. Circuits Syst. II, Exp. Briefs*, vol. 64, no. 7, pp. 742–746, Jul. 2017.

[14] K. Chen, T. Lee, and D. Peroulis, "Co-design of multi-band high-efficiency power amplifier and three-pole high-Q tunable filter," *IEEE Microw. Wireless Compon. Lett.*, vol. 23, no. 12, pp. 647–649, Dec. 2013.

[15] D. M. Pozar, *Microwave Engineering*, 3rd ed. New York, NY, USA: Wiley, 2005.

[16] S. Chen and Q. Xue, "A class-F power amplifier with CMRC," *IEEE Microw. Wireless Compon. Lett.*, vol. 21, no. 1, pp. 31–33, Jan. 2011.

[17] Y. C. Li, K. C. Wu, and Q. Xue, "Power amplifier integrated with bandpass filter for long term evolution application," *IEEE Microw. Wireless Compon. Lett.*, vol. 23, no. 8, pp. 424–426, Aug. 2013.

[18] W. Feng, Y. Shi, X. Y. Zhou, X. Shen, and W. Che, "A bandpass push-pull high power amplifier based on SIW filtering balun power divider," *IEEE Trans. Plasma Sci.*, vol. 47, no. 9, pp. 4281–4286, Sep. 2019.

[19] T. Feng, K. Ma, Y. Wang, and J. Hu, "Bandpass-filtering power amplifier with compact size and wideband harmonic suppression," *IEEE Trans. Microw. Theory Techn.*, vol. 70, no. 2, pp. 1254–1268, Feb. 2022.